VTT Technical Research Centre of Finland

Space debris detection over intersatellite communication signals

Anttonen, Antti; Kiviranta, Markku; Höyhtyä, Marko

Published in:
Acta Astronautica

DOI:
10.1016/j.actaastro.2021.06.023

Published: 01/10/2021

Document Version
Publisher's final version

Acta Astronautica 187 (2021) 156–166

Contents lists available at ScienceDirect

Acta Astronautica

journal homepage: www.elsevier.com/locate/actaastro

Research paper

Space debris detection over intersatellite communication signals

Antti Anttonen *, Markku Kiviranta, Marko Höyhtyä

VTT Technical Research Centre of Finland Ltd, P.O. Box 1100, FI-90571 Oulu, Finland

ARTICLE INFO

Keywords:
Fifth generation (5G)
High-density constellations
Space-borne radar and communications (SBRC)
Space debris

ABSTRACT

In this paper, we apply a space-borne radar and communications (SBRC) concept for detecting space debris over signals that are designed solely for communication purposes. By using a hidden capability of intersatellite communications signals to act as a radar signal as well, we propose a new approach for debris detection that can be used to address the challenges of long-distance and ground-based detection without introducing a separate space-borne radar infrastructure. The performance of the proposed SBRC approach is evaluated from the two timely perspectives in emerging satellite communications, i.e. high-density constellations and 5G satellites. Several new findings are discovered and demonstrated via sophisticated simulations. These include the effect of system-level cooperation gain in small debris detection and link-level estimation of high-velocity debris motion.

1. Introduction

1.1. Space debris

Modern societies nowadays rely on a number of space-borne digital services. These include digital broadcasting, navigation, data and voice communications, and Earth observation services in various forms. Due to the increasing amount of activities, the space near the Earth is getting more crowded. According to European Space Agency, there are currently 6250 satellites in space of which 3400 are still functioning [1]. Moreover, there are millions of smaller space debris objects orbiting around Earth. Despite of awareness of space debris existence and some precautionary actions, the debris situation is evidently getting worse. The International Space Station has maneuvered several orbital adjustments due to debris just during 2020 while the number of all potential conjunctions at low Earth orbits (LEOs) has doubled in the past four years to about 4000 conjunctions just within one month [2]. The reasons for the excitable number of sources of space debris are evaluated in [3]. Intentional disposal of retired satellites to orbit graveyards and unintentional fragmentation of exploded satellites and rocket bodies are the key debris sources that can keep causing debris in new chain reactions. Since also the density of satellite constellations is simultaneously strongly increasing, the collision risk is becoming a serious threat for future space missions [4].

The main approaches to mitigate the effects of space debris are i) debris creation avoidance, ii) debris collision avoidance, iii) debris removal, and (iv) debris shielding for which survey papers can be found, e.g., in [3,5,6]. While debris removal is in its infancy, various avoidance methods for larger objects and shielding satellites from smaller objects have been routinely used for some time. A proper modeling framework of space debris is required for most debris mitigation approaches and several space debris modeling tools and timely catalogs are maintained for larger objects as a part of space situational awareness systems [7]. Nevertheless, the smaller size objects, say less than 1 cm, are modeled and known mainly statistically. Still, even millimeter-size objects have been observed to cause severe damage to the parts of the satellites that cannot be shielded, e.g. solar panels. Therefore, even if a satellite would be able to continue operation after such collisions with a small object, its functionality can be significantly reduced.

1.2. Debris detection

A key enabler in defending satellites against already existing space debris is being able to detect the presence of debris objects and some essential trajectory features such as range and velocity of the debris object. The debris trajectories at LEOs are not stable in the long run which necessitate continuous updating of space objects' trajectory models. Depending on the selected aforementioned debris mitigation method, the requirements for the debris detection and modeling can vary with respect to timeliness and estimation accuracy.

Space debris detection has been conducted largely using ground-based radars (GBRs) and optical measurements [7,8]. While the GBRs are adequate for relatively large objects (say larger than 10–30 cm depending on the altitude), the detection of smaller size objects becomes difficult from the Earth's surface where a typical detection distance

* Corresponding author.
E-mail addresses: antti.anttonen@vtt.fi (A. Anttonen), markku.kiviranta@vtt.fi (M. Kiviranta), marko.hoyhtya@vtt.fi (M. Höyhtyä).

https://doi.org/10.1016/j.actaastro.2021.06.023
Received 17 February 2021; Received in revised form 20 May 2021; Accepted 14 June 2021
Available online 24 June 2021

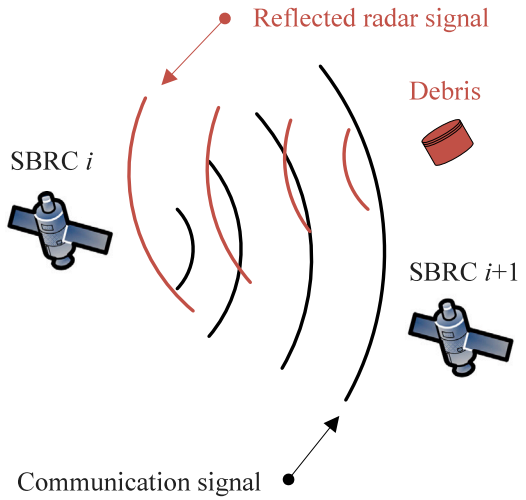

Fig. 1. A simplified illustration of the SBRC concept.

of LEO debris is 500–1000 km. Recently, there have been increasing interest on space-based measurements using impact detectors for submillimeter-size objects and radar or optical detectors for 0.1–10 cm objects [9–11]. For a space-borne radar, a typical detection distance can be as low as 500 m [11]. The benefits of space-borne radars are manifold. That is, it is potentially less sensitive to sunlight, atmospheric distortions, and large signal path losses, unlike the GBRs. However, a separate stand-alone space-borne debris detection system would not be a cost- or spectral-efficient solution as dedicated frequency bands and launches are required if separate radar signals are generated merely for debris detection. As a result, there is a strong need to build complimentary space-borne radar systems that would be more deeply integrated in the emerging satellite communication infrastructure. Since new satellites are launched to the LEOs with burgeoning rate by several satellite operators, e.g. SpaceX, this potential is now more timely than ever before.

1.3. Main contributions

In this paper, we propose a novel space-borne radar and communications (SBRC) approach for space debris detection that addresses the aforementioned challenges related to the fundamental detection accuracy limitation of distant GBRs and the efficiency of a stand-alone space-borne radar system. A simplified illustration is shown in Fig. 1. Specifically, we apply the radar and communication concept for detecting space debris over signals that are designed solely for communication purposes. The SBRC uses a hidden capability of communications signals to act as a radar signal as well and can readily be used to complement legacy space situational awareness system. Although the concept of combining radar and communications is not new in general, to the best of authors' knowledge, its application to space debris detection with satellite communication systems has not been considered before in the open literature. While being used in several terrestrial applications [12–15], such as autonomous vehicles, the application of the radar and communication to space-borne debris detection is far from being trivial. The reasons are the following. The relative speed of debris objects can be in the level of 15 km/s which is several magnitudes more than the maximum speed of terrestrial radar objects. Furthermore, the object sizes can be much smaller while the detection space is much larger than in typical terrestrial sensing applications.

Based on the above observations, we evaluate the performance of the SBRC approach from two timely perspectives in emerging satellite communications: high-density constellations and 5G satellites. Several new findings are discovered and demonstrated via sophisticated simulations. These include the effect of cooperation in debris detection with high-density constellations and the radar estimation accuracy with high-velocity debris movement. Moreover, we develop a novel estimator that jointly estimates the velocity and range of a very high speed debris object, following the 5G communication signal structure. The main benefits of the approach are that a separate space-borne radar infrastructure would not be needed, the payload of a satellite can be reduced, and the spectrum efficiency is improved. In this work, we want to avoid any changes to satellite communication signals resulted from introducing the SBRC approach to enable an ease integration into satellite systems. Therefore, similar to [16], we focus on the radar performance instead of the communications performance because we use existing communication signals to detect debris rather than aim at jointly optimizing both radar and communication domains. Furthermore, there is already quite extensive literature treating 5G nonterrestrial communications and its performance, see [17–22].

The rest of the paper is organized as follows. First, the proposed SBRC concept for debris detection is described in Section 2. Then, cooperative debris detection approaches and performance evaluation at a system level are provided in Section 3. In Section 4, we present the 5G-SBRC principles at a link level and propose approaches to the high-velocity debris parameter estimation. Finally, we provide our conclusions in Section 5.

2. Proposed concept for space debris detection

2.1. System functionality

The proposed SBRC concept for debris detection is illustrated in Fig. 2 from two different viewpoints. The black diamonds represent SBRC-enabled satellites which orbit around the Earth in different controlled constellation orbit planes and the red stars denote the space debris that follow their own uncontrolled orbits independent of the satellite constellations. The SBRC module consists of the three main parts: communication transmitter (CTX), communication receiver (CRX), and radar receiver (RRX). The communication is needed for satellite-ground links and intersatellite links (ISLs). In this work, we focus on using ISL communication signals for radar tasks but the inclusion of the satellite-ground links is also possible. The CTX generates a communication signal that is used to relay data between satellites via ISLs and the CRX receives the data signal from the ISLs that it is connected to. The RRX is responsible of radar signal preprocessing tasks before the presence of a debris object can be detected and further parameters, such as range and velocity, to be estimated. A distinctive preprocessing task for the RRX is to allow radar sensing with modulated data which necessitates the removal of the data modulation before the debris detection can take place. Since the RRX receives a reflected signal transmitted by the CTX, the data modulation can be removed with the help of the CTX that is located in the same SBRC module as the RRX, see Fig. 2.

2.2. Preliminary assessment of operational conditions

The debris illumination capability of the SBRC, which is measured with the radar cross section (RCS), defines largely the amount of reflected power from a detected object. Regarding our SBRC approach, the RCS depends essentially on the used carrier frequency of the satellite communication signal in relation to the target debris shape. The RCS (given in m^2) can be determined for a typically assumed sphere-shaped debris as a Mie series function as well as a high-frequency asymptotic approximation [23]. Fig. 3(a) illustrates the effect of carrier frequency on the RCS with different debris sizes d_{deb}. Clearly, for the debris size in the vicinity of 1 mm, the carrier frequency of the SBRC system must be tens of GHz to avoid significant signal attenuation in the power reflection process while for larger debris sizes smaller carrier frequencies may be sufficient.

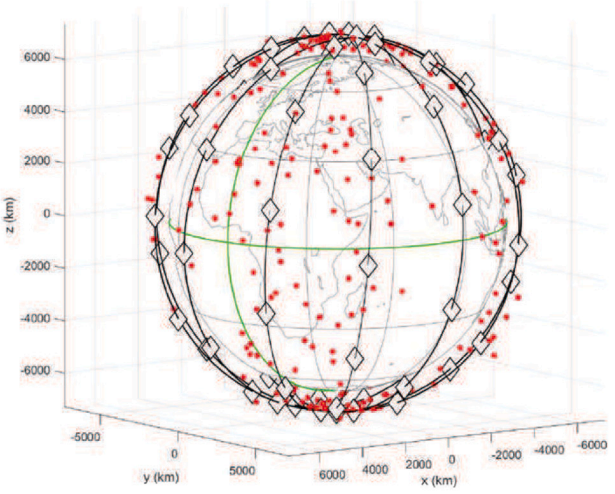

(a) Overall system view.

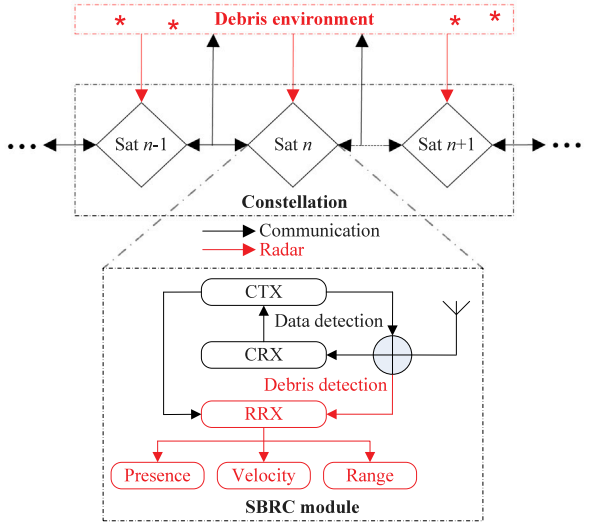

(b) SBRC view.

Fig. 2. The proposed SBRC concept for space debris detection. Diamonds and stars denote satellites and debris, respectively. The SBRC modules include the communication transmitter (CTX), communication receiver (CRX), and radar receiver (RRX).

An important operation condition is the achievable signal-to-noise ratio (SNR) at the SBRCs before the debris is detected. Depending on the depth that target system parameters are integrated into the SNR equation and the selected channel environment, different forms of an SNR may exist. We focus on the free space propagation environment that is a valid assumption for space-borne radar detection [11]. The received SNR in a free space propagation environment is given in a common format as [23, p. 30]

$$\gamma = \frac{P_{\mathrm{tx}} G_{\mathrm{tx}} G_{\mathrm{rx}} \lambda^2 \epsilon \upsilon}{(4\pi)^3 r^4 k_{\mathrm{B}} T F L} \tag{1}$$

where P_{tx} is the transmission power, G_{tx} and G_{rx} are, respectively, the transmit and receive antenna gains, $\lambda = c/f_{\mathrm{c}}$ is the signal wavelength, c is the speed of light, f_c is the carrier frequency, υ is the message length used for detection, r is the detection range, k_{B} is the Boltzmann's constant, T is the temperature, F is the noise figure, and L is the system loss. For a parabolic antenna, $G_{\mathrm{tx}} = G_{\mathrm{rx}} = \eta_{\mathrm{ant}} \pi^2 d_{\mathrm{ant}}^2 / \lambda^2$ where η_{ant} and d_{ant} are the antenna efficiency and diameter, respectively. Fig. 3(b) provides an SNR comparison for detecting 1 mm and 20 mm space debris with a millimeter-wave and low-power SBRC ($P_{\mathrm{tx}} = 50$ W, $d_{\mathrm{ant}} = 0.8$ m, $f_{\mathrm{c}} = 60$ GHz) and a typical (cf. [7]) ultra-high frequency and high-power GBR ($P_{\mathrm{tx}} = 1$ MW, $d_{\mathrm{ant}} = 34$ m, $f_{\mathrm{c}} = 1.3$ GHz). A sufficient SNR must be achieved at the detector, say at least 10 dB, and the corresponding detection range (showed with red dashed line in Fig. 3(b)) must be supported by the particular SBRC technology. It is seen that while the GBRs may perform better than the SBRCs as a function of detection range due to a very high transmission power and large antenna size, the GBRs have a challenge to detect small debris because they cannot get sufficiently close to the debris objects from the Earth surface (i.e. $r \geq 500$ km) similar to an SBRC system that is located in the space. Moreover, this simplified comparison neglects any atmospheric attenuation that may further impair the performance of GBRs.

The ISL distance as function of number of satellites in the constellation is given for intraplane and interplane links in [24]. In practice, the satellites cannot be brought arbitrarily close to each other either due to cost, safety, and interference regulations. It is then clear that there will always be instantaneous spatial gaps for detecting very small space debris with an SBRC whose detection distance is limited as illustrated in Fig. 3(b). Fortunately, this can be mitigated by introducing satellite cooperation for debris detection. The effects of the number of satellites and planes are further analyzed for the cooperative debris detection performance in Section 4.

The communication signal of the 5G new radio is essentially based on the cyclic prefix orthogonal frequency division multiplexing (CP-OFDM) approach which is currently considered to be used e.g. in 5G terrestrial vehicular-to-vehicular applications as well as in emerging 5G nonterrestrial networks [15,17]. The fundamentals of the CP-OFDM approach is omitted here and we refer to [16,25–28] to find more detailed information. We instead focus on some important consequences of using CP-OFDM signal for the proposed SBRC concept (denoted hereafter as a 5G-SBRC system) that must be well understood by a system designer. The two limiting factors is to preserve the orthogonality of subcarriers and to ensure unambiguity of range and velocity estimations. Specifically, while proved to be quite advantageous for the communications domain, the CP-OFDM signal structure limits the SBRC performance in the debris estimation domain in the following ways.

Firstly, the debris range is estimated by measuring the total time it takes for the 5G-SBRC signal to make the round trip between the target debris and a measuring SBRC. To preserve the subcarrier orthogonality, the time delay τ is limited by the length of the cyclic prefix T_{cp} of the CP-OFDM signal. On the other hand, the maximum unambiguous range presumes that $\tau \Delta f < 1$ where Δf is the subcarrier spacing. Consequently, the maximum possible debris detection range for the 5G-SBRC is readily given as

$$r_{\max} = \min\left(\frac{c}{2\Delta f}, \frac{cT_{\mathrm{cp}}}{2}\right). \tag{2}$$

Secondly, the velocity υ of a debris object can be estimated by estimating the corresponding Doppler shift of the reflected signal as $f_{\mathrm{D}} = 2\upsilon f_{\mathrm{c}}/c$. The estimation of debris velocity is unambiguous only if $2|T_{\mathrm{sym}} f_{\mathrm{D}}| < 1$ where T_{sym} is the total symbol duration of the CP-OFDM signal. Furthermore, the residual allowed frequency offset must be small in relation to the subcarrier spacing to preserve the orthogonality of the subcarriers of the CP-OFDM signal. The maximum velocity without any frequency offset compensation is, therefore, defined as

$$\upsilon_{\max} = \min\left(\frac{c}{2T_{\mathrm{sym}} f_{\mathrm{c}}}, \frac{c\beta\Delta f}{2f_{\mathrm{c}}}\right) \tag{3}$$

where $\beta \ll 1$ is a selected constant (typically $\beta = 0.1$) to ensure a sufficient signal quality with residual frequency offsets (cf. [25]).

Some numerical values are illustrated in Table 1 for the selected 5G signal modes. While a typical space-based debris detection range target of 500 m (cf. [11]) can be satisfied with several signal modes, the debris estimation with high velocities is challenging for the 5G-SBRC.

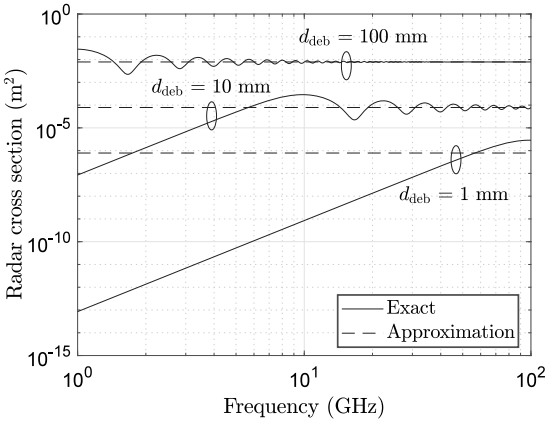

(a) Effect of carrier frequency on the RCS.

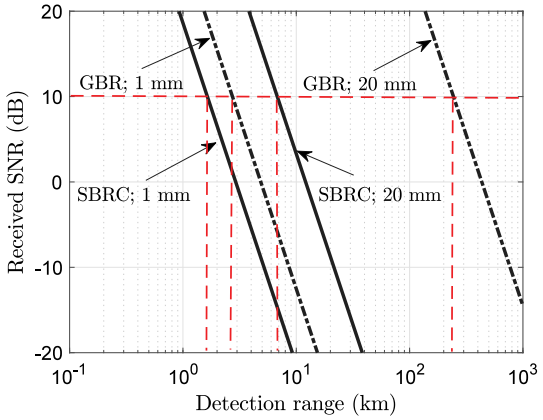

(b) Effect of range on the SNR. The red dashed lines exemplify the ranges that lead to the SNR of 10 dB.

Fig. 3. Illustration of effects of system parameter selections.

Table 1
Signal parameters and resulted conditions for different 5G system modes.

Parameter	5G 20	5G 50	5G 100	5G 400
Bandwidth (MHz)	20	50	100	400
Carrier frequency (GHz)	64.8	64.8	64.8	64.8
Subcarrier spacing (kHz)	15	60	60	120
Cyclic prefix[a] (us)	4.7	4.2	4.2	0.59
Symbol duration (us)	71.4	20.8	20.8	8.9
Max range (m)	705	625	625	88
Max velocity[b] (m/s)	3.5	13.9	13.9	27.8

[a]Represents max possible cyclic prefix per mode.
[b]Without Doppler offset compensation.

This is because the maximum relative debris speed of 15 km/s at the LEO orbit is about 100 times larger than the highest mobility of 500 km/h (138 m/s) experienced in typical terrestrial vehicle-to-vehicle applications. As a result, in Section 4, we revisit the frequency offset compensation problem and present a novel compensation approach that jointly estimates the velocity and range of the target debris object while supporting orbitals speeds of up to 15 km/s.

3. Debris detection with limited coverage: System-level cooperation

The evaluation of operational conditions of the proposed SBRC concept in Section 2 indicates that the detection of mm-size debris objects is still challenging even though the SBRCs are brought much closer to the orbiting debris compared to GBRs. This is because the transmission powers and antenna diameters of any space-borne radar have to be much smaller, thus limiting the radar coverage. Nevertheless, the SBRC concept provides an appealing opportunity for cooperation within respective constellation structures. In this section, our goal is to present potential cooperative debris detection approaches and provide some initial estimates about cooperation gain in different satellite communication constellation settings. In a conventional radar system, a single radar can perform multiple estimates to achieve integration gain to significantly improve the detection performance. In the SBRC concept, the satellite constellations with detection capability and debris objects have in general different orbits where the relative speed can be up to 15 km/s. As a result, there is a very limited time to obtain integration gain using just separate detections from isolated satellites with SBRC capability.

As mentioned in Section 2, the detection of debris presence is the first operational objective of the SBRC. After the presence is detected, its range and velocity of debris objects can be estimated. In this section we focus on the debris presence detection. In order to evaluate the potential gain in cooperatively detecting the space debris for the methods proposed in the previous subsection, we use a simplified signal model to enable performance analysis with large constellations and high time resolution. In other words, in this system-level study the main aim is to reveal the potential cooperative detection gain rather than to include all nonidealities taking place at the link level that prevent performance evaluation for large constellation sizes due to exponentially increased complexity. We then add more details to the link-level model in Section 4 to study the estimation performance of individual links more carefully via link-level simulations.

3.1. Cooperative detection methods

Consider SBRC-enabled satellites communicating with each other via intersatellite links and moving along the trajectories of given orbits of the target constellation. Debris objects have their own orbit trajectories independent of the satellite orbits. It is assumed that different debris objects are sufficiently separated in the space so that the measurements are distinguishable and arrive at different time intervals. Since the debris density in the orbits is typically relatively low in relation to a typical detection range of small objects for a single satellite, this assumption is valid.

Let $r_{ik} = s_{ik} + n_{ik}$ denote a complex sensing measurement made in the ith SBRC-enabled satellite at a discrete time index k where s_{ik} is the received phase-modulated satellite communication signal in the ith satellite reflected from a debris object at time index k, and n_{ik} is the complex white Gaussian noise term with given noise power and corresponding indexing. The cooperative detection constructs independent measurements from an object and the measurements are combined as $q = f(r_{ik})$ where $f(\cdot)$ denotes a selected combining function. Finally, using a combined measurement q a decision about debris object presence is made using statistical hypothesis testing. The null hypothesis H_0 assumes that a target is not present, i.e., $s_{ik} = 0$. The second hypothesis H_1 assumes that the target is present and the signal is given as $s_{ik} = a_{ik}\exp(j\phi_{ik})$ where a_{ik} and ϕ_{ik} are, respectively, the received signal amplitude and phase in the ith satellite at time index k. The hypothesis H_1 is assumed to be true if $\mathrm{Re}(q) > T_\mathrm{d}$, where $\mathrm{Re}(x)$ is the real part of x and T_d is the selected detection threshold, while hypothesis H_0 is true otherwise. The threshold is typically selected to preserve a target probability of false alarms. In practice, a separate sharing procedure is needed to collect all the relevant measurements at a selected fusion satellite where the combining takes place. Implementation details of this procedure are out of the scope of this paper but existing intersatellite links of satellite constellations provide a suitable information sharing platform for that purpose.

We consider a correlation-based coherent detection in time domain (cf. [29]). Extensions to other detection approaches, such as the fast Fourier transform-based detector studied in Section 4, is also possible. The decision statistics are formed with one of the three cases, namely noncooperative detection, pre-detection cooperation, and post-detection cooperation. For the noncooperative case, no combining is used and $q_\mathrm{non} = r_{ik}s_{ik}^*, \forall i,k$. In case of pre-detection cooperation, the decision variable is presented as $q_\mathrm{pre} = \sum_{ik} r_{ik}s_{ik}^*$. Let z_{ik} be a binary sequence of the noncooperative decision tests $\mathrm{Re}(r_{ik}s_{ik}^*) > T_\mathrm{d}, \forall i,k$. Then, the post-detection decision statistics become $q_\mathrm{post} = \sum_{ik} z_{ik}$ where $q_\mathrm{post} \geq 1$ leads to assume H_1 and H_0, otherwise. The SBRC cooperation concept is further illustrated in Fig. 4.

Clearly, making noncooperative decisions is the easiest approach as no sharing of detected data between satellites is needed. Moreover, sharing binary information for the post-detection cooperation between different satellites would be easier than sharing full correlation results as in the pre-detection approach. Obviously, the sharing process also causes extra delay to the availability of the detection decision. The relative detection performance of these methods, in particular the achievable cooperation gain, is then of high interest and addressed next in Section 3.2, first analytically and then with Monte Carlo simulations.

3.2. Performance analysis

3.2.1. Orbital mechanics

From the SBRC's detection performance point of view, an important characteristic is the dynamics of relative positions of satellites and space debris. The dynamic Earth-centered 3D position $\mathbf{p}_k$ in space at time index k can be found, e.g., via elliptic Kepler orbits, as [7]

$$\mathbf{p}_k = \begin{pmatrix} x_k \\ y_k \\ z_k \end{pmatrix} = \begin{pmatrix} \eta_k \cos(u_k)\cos(\Omega_\mathrm{R}) - \eta_k \sin(u_k)\sin(\Omega_\mathrm{R})\cos(\zeta) \\ \eta_k \cos(u_k)\sin(\Omega_\mathrm{R}) + \eta_k \sin(u_k)\cos(\Omega_\mathrm{R})\cos(\zeta) \\ \eta_k \sin(u_k)\sin(\zeta) \end{pmatrix} \quad (4)$$

where ζ is the orbit inclination, Ω_R is the right ascension of the ascending orbit node (RAAN), and η_k and u_k are, respectively, the orbit radius and the argument of true latitude at time index k. The time-variant parameters η_k and u_k depend on the current orbital position as well as on the orbit eccentricity and semimajor axis. The model is considered as a sufficient approximation especially for shorter time frames where gradually increasing cumulative effects from nonideal perturbations, such as atmospheric drag, do not yet affect significantly. Nevertheless, the proposed SBRC framework supports also more involved orbit models. Using Eq. (4), the range between the ith satellite position $\mathbf{p}_{ik}^\mathrm{sat}$ and a debris object position $\mathbf{p}_k^\mathrm{deb}$ at each time index k is then found as $r_{ik} = \left\|\mathbf{p}_{ik}^\mathrm{sat} - \mathbf{p}_k^\mathrm{deb}\right\|$.

Another important characteristics is whether a satellite has visibility to a debris object that may be hindered by the Earth's curvature. If there is no visibility, the reflected signal power from a debris object is zero. By applying the results from [30], the visibility function between the ith satellite and a debris object at time index k can be determined as

$$\theta_{ik} = \cos^{-1}\left(\frac{r_\mathrm{E}}{\left\|\mathbf{p}_{ik}^\mathrm{sat}\right\|}\right) + \cos^{-1}\left(\frac{r_\mathrm{E}}{\left\|\mathbf{p}_k^\mathrm{deb}\right\|}\right) - \cos^{-1}\left(\frac{\mathbf{p}_{ik}^\mathrm{sat}\cdot\mathbf{p}_k^\mathrm{deb}}{\left\|\mathbf{p}_{ik}^\mathrm{sat}\right\|\left\|\mathbf{p}_k^\mathrm{deb}\right\|}\right) \quad (5)$$

where r_E is the Earth's radius. If $\theta_{ik} > 0$, the visibility between the ith satellite and debris object exists at time index k.

3.2.2. Analytical methods

In general, the received signal at an SBRC-enabled satellite reflected from a debris object is a time-varying variable due to noise, orbital dynamics, and fluctuating radar cross section. The average detection probability for the noncooperative detection with a single measurement is given as

$$P_\mathrm{d} = \int_0^\infty P_\mathrm{d}(\gamma)p(\gamma)d\gamma \quad (6)$$

where γ is the instantaneous signal-to-noise ratio (SNR), $P_\mathrm{d}(\gamma)$ is the detection probability conditioned on γ, and $p(\gamma)$ is the pdf of γ. The conditional detection probability depends on the selected detection structure and system assumptions [29,31]. For the coherent detection, $P_\mathrm{d}(\gamma) = \mathrm{erfc}\{\mathrm{erfc}^{-1}(2P_\mathrm{fa}) - \sqrt{\gamma}\}/2$ where $\mathrm{erfc}(\cdot)$ is the complementary error function and P_fa is the target false alarm probability. In case of pre-detection cooperation, γ can also represent the SNR at the output of the combiner and (6) applies directly. In case of post-detection cooperation, $P_\mathrm{d}^{(i)}$ is first obtained from (6) for the ith SBRC and the overall detection probability becomes $1 - \prod_i (1 - P_\mathrm{d}^{(i)})$. The corresponding false alarm probability is given as $1 - \prod_i (1 - P_\mathrm{fa}^{(i)})$ where $P_\mathrm{fa}^{(i)}$ denotes the target false alarm probability for the ith SBRC before combining.

However, for the target dynamic orbital mechanics and cooperative combination approaches, the pdf $p(\gamma)$ is unknown in a closed form, hindering the use of pure analytical approach. One approach is to use a semi-analytic method which provides a discrete approximation of $p(\gamma)$ by simulating the target orbital geometry realizations while using the available analytical form for $P_\mathrm{d}(\gamma)$. The semi-analytic approach can be used to reduce the complexity of full Monte Carlo simulations which may be infeasible for very large satellite constellations.

3.2.3. Simulation results

In this section, the objective is to compare the detection performance for the noncooperative and cooperative detection approaches presented in the previous subsections. In addition of making the typical assumption that the detected object is collocated within certain range from the radar device, we also allow the debris to be placed randomly in the selected SBRC constellation surface and evaluate the average detection probability with different detection configurations within a limited observation time. This basis provides important information on the debris detection capability from the system-level point of view. To obtain insight about potential upper limits on the cooperation gain, we assume a continuously directed beam from the closest SBRCs to a

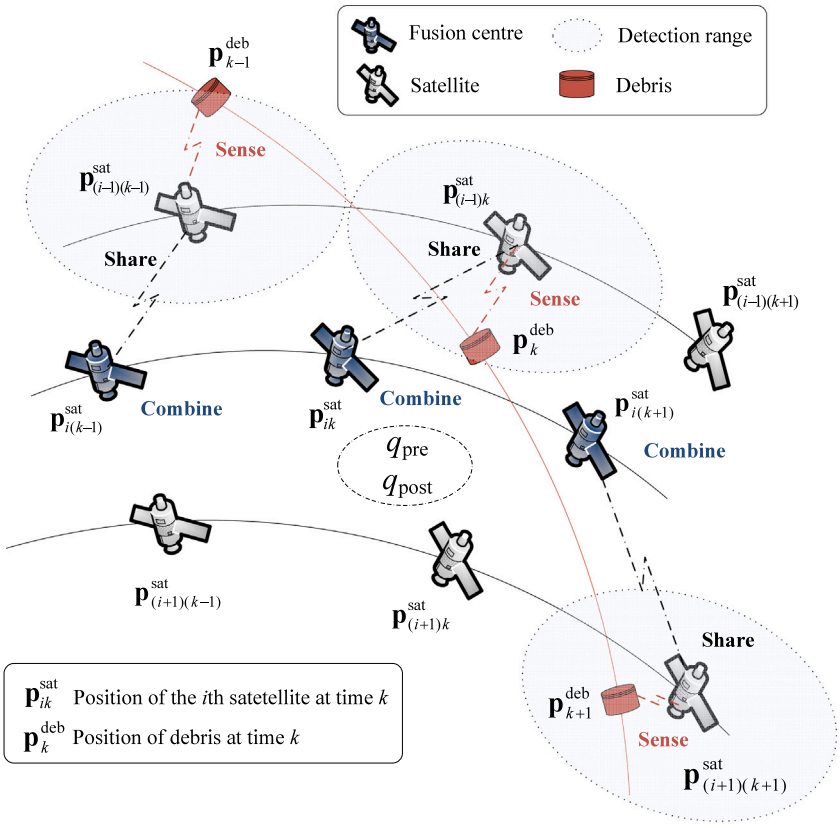

Fig. 4. Illustration of cooperative detection with an SBRC-enabled satellite constellation.

Table 2
SBRC parameters.

Parameter	Value
Message length	1 ms
System losses	2 dB
Noise figure	3 dB
Noise temperature	297 K
Observation time	1.5 h
Carrier frequency	60 GHz
Antenna efficiency	0.7
Path loss	Free space
Data modulation	QPSK
Satellite constellation type	Walker
Orbit altitude	500 km
Eccentricity	Circular
Inclination	60 deg

Table 3
Debris parameters.

textbfParameter	Value
Debris type	Metal sphere
RCS fluctuation	Exponential
Altitude	500 km
Eccentricity	Circular
Inclination	−90–90 deg (random)
RAAN	0–360 deg (random)
Initial true anomaly	0–360 deg (random)

sphere-shaped debris object without nonideal scan and channel estimation losses. The nonideal estimation assumptions are then investigated in the more detailed link-level studies in Section 4. The main simulation parameters are summarized in Tables 2 and 3 for the target SBRC system and debris model, respectively.

We first aim at illustrating the effect of some key system parameters for detection performance in a simpler environment to obtain some inference on different satellite capabilities to detect space debris at a static distance without dynamic orbital movements or RCS fluctuation. For this purpose, we define three satellite classes regarding the transmission power P_{tx} and antenna diameter d_{ant}. Class 1 uses $P_{\text{tx}} = 100$ W and $d_{\text{ant}} = 1$ m representing a relatively large satellite. Class 2 uses $P_{\text{tx}} = 10$ W and $d_{\text{ant}} = 0.5$ m. Class 3 then applies $P_{\text{tx}} = 1$ W and $d_{\text{ant}} = 0.1$ m which are typical values for smaller nanosatellites. Fig. 5 shows the detection performance in the noncooperative mode using a single measurement for different satellite classes, false alarm probabilities, and static distances as function of debris size. It is seen that, as could be reasonably expected, the selected satellite class has a significant effect on the detection performance and largely defines the relationship between detectable debris size and detection distance. As in this setup the distance and the received SNR are static, the conditional analytical results from Section 3.2.2 apply.

Next, Fig. 6 shows the mean detection performance for different cooperation modes as function of debris diameter with different time and spatial resolutions. Parameters T_{rt}, N_{c}, and N_{p} denote the message repetition time, total number of satellites in the constellation, and number of orbital planes, respectively. Here we have selected Class 1 satellites which target $P_{\text{fa}} = 0.01$. Unlike in Fig. 5, in this case, the space debris is randomly placed on constellation surface and the relative distances between satellites and space debris are time-varying during the observation time interval, as described in Section 3.2.1. It is observed that (i) cooperation can provide significant gain for the detection performance, (ii) post-detection cooperation is superior for small debris while pre-detection cooperation has similar or superior performance for larger debris after the received SNR is sufficient to obtain additional gain from the measurement fusions before detection, and (iii) increase of spatiotemporal sensing resolution can improve the performance significantly with spatial resolution (see Figs. 6(d)–6(f) for up to 10 000 satellites per constellation) being often more effective to bring the measuring SBRCs close enough to small debris. Finally, it is

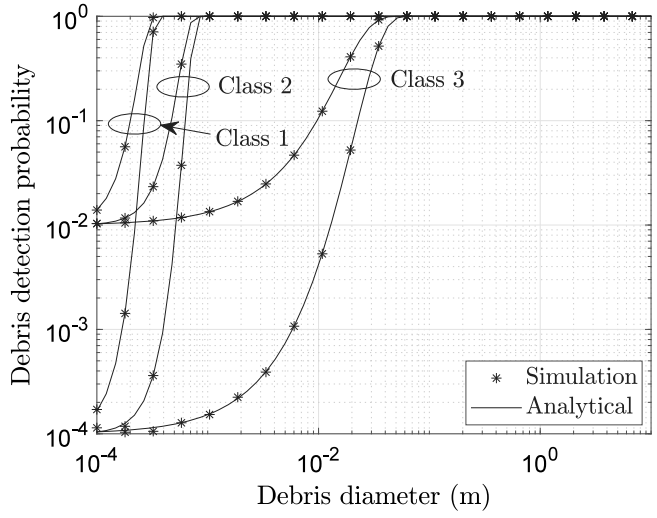

(a) 500 m

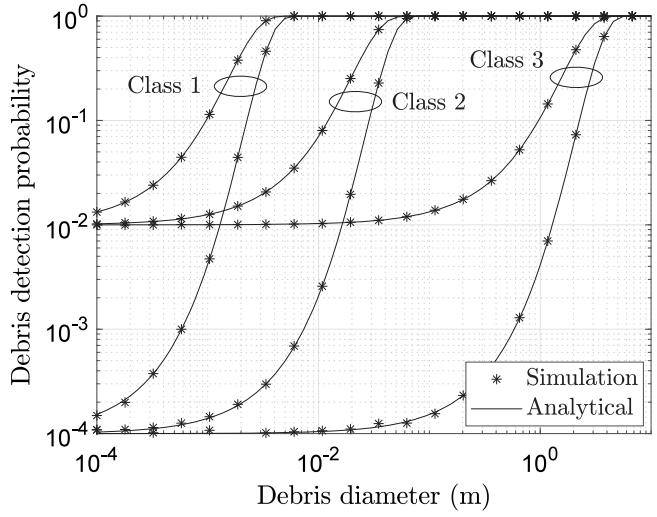

(b) 5000 m

Fig. 5. Performance with fixed detection ranges (500 m and 5000 m) and without cooperation for different satellite classes. Upper and lower curves for each class represent target $P_{fa} = 0.01$ and $P_{fa} = 0.0001$, respectively.

seen that the semi-analytic approach from Section 3.2.2 follows closely the corresponding Monte Carlo simulation results.

4. Debris parameter estimation with high velocity: Link-level 5G signaling

In the previous section, we addressed system level performance and potential gain of detecting debris cooperatively. In this section, we focus more on the link-level issues and actual estimators of key debris parameters. First, the 5G-SBRC model is described. Then, we propose an estimator which jointly estimates the velocity and range of the target debris object while supporting relative debris speeds of up to 15 km/s. Finally, the performance results are summarized.

4.1. Link-level 5G-SBRC model

Fig. 7 illustrates the target link-level 5G-SBRC model. In the figure, communication transmitter (TX) and receiver (RX) blocks are presented in blue and the radar receiver blocks for the debris detection are presented in green. The model involves both the physical downlink (PD) and the physical uplink (PU) with a shared channel (SCH). The model generates a transport block, downlink (DL) or uplink (UL) channel codeword, and maps the complex symbols to the resource grid. The DL transmitter model includes demodulation reference signals (DM-RS), phase tracking reference signals (PT-RS), and synchronization signal (SS) bursts. The UL transmitter model includes DM-RS. The CP-OFDM (de)modulation is performed via fast Fourier transform (FFT) and inverse FFT (IFFT). A separate timing synchronization is needed only for the communication task.

The transmitted Grid X and the received Grid Y, which are generated for the debris detection and illustrated in Fig. 7 with orange, are frequency domain matrices of size $N_{sc} \times N_{sym}$ where N_{sc} is the number of subcarriers and N_{sym} is the number of OFDM symbols used for the estimation. The resulting radar processing gain from the periodogram-based estimation is then $10\log_{10}(N_{sc}N_{sym})$ dB. The received grid sample in the pth row and the qth column can be expressed as

$$Y_{pq} = X_{pq} \exp\left[j2\pi(qT_{sym}f_D - p\tau\Delta f)\right] + \Omega_{pq} \tag{7}$$

where X_{pq} is the known transmitted signal, τ is the delay, Ω_{pq} denotes the complex additive white Gaussian noise, and the other parameters were defined in Section 2.2.

In the radar part of the SBRC receiver, the division operation between the transmitted and received signals first removes the effect of data modulation used for communications. As a result, we obtain the input signal $G_{pq} = Y_{pq}/X_{pq}, \forall p, q$, for the periodogram-based estimator which is treated next.

4.2. Range and velocity estimation with high object velocities

When the frequency of the local oscillator does not match with the received signal, a carrier frequency offset δf will appear. The frequency difference is created by the oscillator imperfections and the Doppler shift. A framework for the frequency-domain range-velocity estimation is given by [16,28,32] in the presence of ICI which is sufficient for relatively low target object velocities without the need for Doppler offset compensation. However, in debris detection much higher frequency offset must be treated.

The frequency offset, relative to the subcarrier spacing, can be subdivided as [27,33]

$$\xi = \frac{\delta f}{\Delta f} = I + \varphi \tag{8}$$

where $0 \le I \le I_{max}$ and $-1/2 \le \varphi < 1/2$ are the integer frequency offset (IFO) and fractional frequency offset (FFO), respectively. Parameter I_{max} is determined by the maximum expected frequency offset. For a Doppler-induced offset, $I_{max} = \lfloor f_D/\Delta f \rfloor$. The IFO has the following two effects on the received signal after the FFT which must be compensated. First, the signal transmitted on subcarrier p is received on subcarrier

$$p + I \tag{9}$$

due to the cyclic shift. Secondly, there is a phase change proportional to the OFDM symbol index q as

$$\delta\phi = \frac{2\pi I q N_{cp}}{N_{fft}} \tag{10}$$

where N_{cp} and N_{fft} are the sample lengths of the CP and FFT, respectively. These two phenomena must be compensated before the periodogram calculation can provide a useful output.

As seen from Fig. 7, the range and velocity estimations are performed through the periodogram over the Grid G by taking first the FFT over the OFDM symbols (column by column) and then over the subcarriers (row by row). Let $N_1 \ge N_{sym}$ and $N_2 \ge N_{sb}$ denote the number of possible range profiles n and velocity profiles m, respectively.

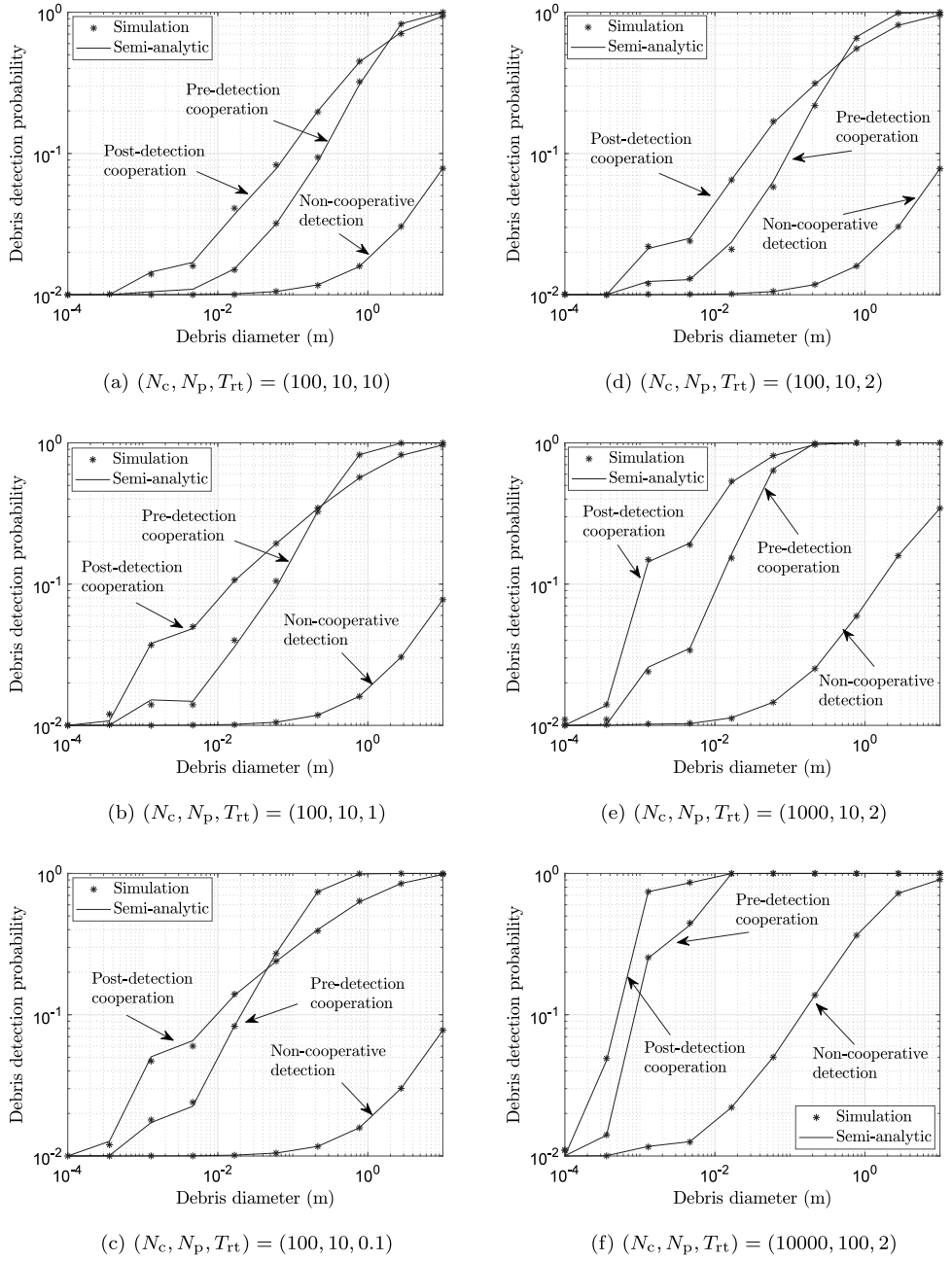

(a) $(N_c, N_p, T_{rt}) = (100, 10, 10)$

(b) $(N_c, N_p, T_{rt}) = (100, 10, 1)$

(c) $(N_c, N_p, T_{rt}) = (100, 10, 0.1)$

(d) $(N_c, N_p, T_{rt}) = (100, 10, 2)$

(e) $(N_c, N_p, T_{rt}) = (1000, 10, 2)$

(f) $(N_c, N_p, T_{rt}) = (10000, 100, 2)$

Fig. 6. Performance with dynamic orbital mechanics and cooperation. Subfigures a–c show the temporal effect (T_{rt} varies) while d–f show the spatial effect (N_c and N_p vary).

The periodogram-based maximum likelihood estimators for the range and velocity are, respectively, obtained as

$$\hat{r} = \frac{\hat{\tau} c}{2} = \frac{\hat{n} c}{2 N_{\text{fft}} \Delta f}, \tag{11}$$

$$\hat{v} = \frac{\hat{f}_D c}{2 f_c} = \frac{\hat{m} c}{2 N_{\text{fft}} T_{\text{sym}} f_c} \tag{12}$$

where

$$(\hat{n}, \hat{m}) = \arg \max_{n,m} \left| \sum_{p=0}^{N_1-1} \left(\sum_{q=0}^{N_2-1} G_{pq}(I) \Theta(q, I) \exp\left(\frac{-j2\pi qm}{N_2} \right) \right) \exp\left(\frac{j2\pi pn}{N_1} \right) \right|^2, \tag{13}$$

$$G_{pq}(I) = \frac{Y_{(p+I)q}}{X_{pq}}, \tag{14}$$

$$\Theta(q, I) = \exp\left(\frac{-j2\pi I q N_{\text{cp}}}{N_{\text{fft}}} \right). \tag{15}$$

Through (13)–(15), we have modified the low-velocity approach of [32] to jointly include the IFO into range and high-velocity estimations without the need to estimate the IFO component explicitly. Specifically, the IFO is jointly compensated by performing the periodogram maximization conditioned on all possible integers I and by taking into account the corresponding cyclic and phase shifts in (9) and (10). Since both (14) and (15) retain the finite candidate value sets, the approach is appealing also from an implementation point of view. In essence, the proposed method enables a high-speed range-velocity estimator of the debris object which was one of the main objectives of this paper.

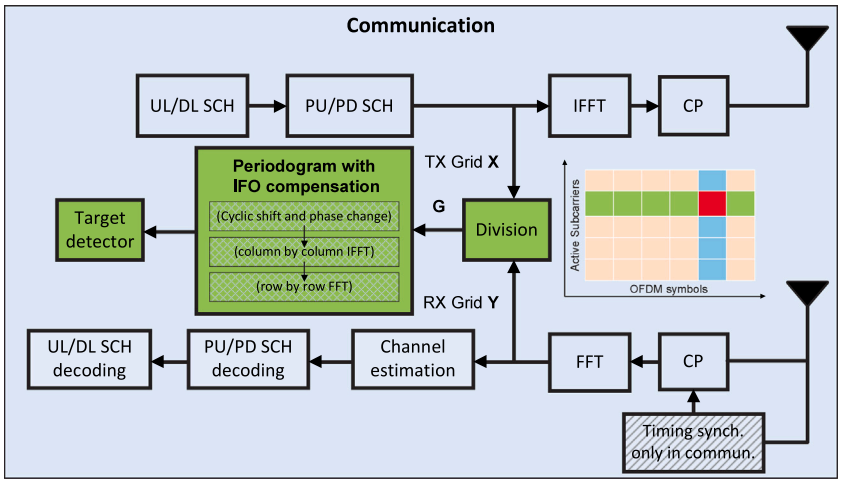

Fig. 7. Link-level model for 5G-SBRC.

Table 4
Parameters and resulted RMSE bounds for different 5G system bandwidths.

Parameter	5G 20	5G 50	5G 100	5G 400
Bandwidth (MHz)	20	50	100	400
Carrier frequency (GHz)	64.8	64.8	64.8	64.8
Subcarrier spacing (kHz)	15	60	60	120
Number of subcarriers	1200	792	1584	3168
Number of symbols	64	256	128	512
Processing gain (dB)	49	53	53	62
Range RMSE bound (m)	2.4	0.9	0.5	0.1
Velocity RMSE bound (m/s)	0.16	0.16	0.31	0.16

4.3. Performance results

4.3.1. Analytical methods

In this subsection, we first intend to analyze the accuracy of the joint range and velocity estimator presented in the previous subsection. The selected criterion is the commonly used root mean square error (RMSE). Based on the theoretical uniform error distribution, the lower bound for the RMSE of the range and velocity estimation is given as (cf. [16])

$$\chi = \sqrt{\frac{\Psi^2}{12}} \tag{16}$$

where Ψ denotes the resolution of the estimator. Specifically, for the range and velocity $\Psi = c/(2\Delta f N_{\mathrm{sc}})$ and $\Psi = c\Delta f/(2N_{\mathrm{sym}} f_{\mathrm{c}})$, respectively. The calculated lower bounds of the RMSEs are presented in Table 4.

4.3.2. Simulation results

Using the 5G-SBRC model in Fig. 7, the simulated RMSE results are provided in Figs. 8(a) and 8(b) for the range and velocity estimations, respectively. For brevity, the 5G 100 signaling mode is used as an example. The cases, where only FFO is present and then both FFO and IFO are present with the proposed IFO compensation method, are illustrated. The SNR values on the x-axis are relatively small because here the SNRs are defined as SNRs per subcarrier. The simulation results demonstrate how the 5G-SBRC approaches the analytical RMSE lower bounds (see Table 4) already for relatively low SNR values. At low SNR, there is also a range of SNR in which the RMSE rises very rapidly as SNR decreases. The SNR at which this effect is first apparent is called the SNR threshold, cf. [34]. It is observed from Figs. 8(a) and 8(b) that with the applied IFO compensation, the RMSE performance is comparable to the case when there is only FFO present as the RMSEs approach the respective lower bounds. The relative SNR degradation is caused by the residual error due to the finite-length IFO compensation from a noised signal. Nevertheless, without the proposed IFO compensation, the RMSE performance would naturally collapse and, in that case, is not meaningful to present for the high velocity debris estimation.

Fig. 9(a) further illustrates the detection probability as a function of SNR per subcarrier. Similarly, to Fig. 9, the detection probability fails also rapidly when the SNR decreases below the SNR threshold. Fig. 9(b) then presents the points for a minimum SNR per subcarrier to achieve the range RMSE lower bound and the maximum range set by the defined cyclic prefix. In more detail, the SNR point (marked as a filled black circle) corresponds the SNR threshold above which the presented estimators work very well. In these results, the free-space path loss model from (1) is assumed with $P_{\mathrm{tx}} = 50$ W, $d_{\mathrm{ant}} = 0.28$, $\eta_{\mathrm{ant}} = 0.7$, $F = 3$ dB, and $L = 2$ dB. Based on the results, we can conclude that the typical targets for space-borne debris detection of 500 m and 15 km/s are achievable with the proposed estimator structure and 5G-SBRC system.

5. Conclusions

In this paper, we propose a new approach for space debris detection by using a hidden capability of satellite communications signals to act as a radar signal as well. The performance of the proposed SBRC approach is evaluated from two timely perspectives in emerging satellite communications, namely high-density constellations and 5G satellites. The work is motivated by the fact that despite of awareness of space debris existence and some precautionary actions, the debris situation near the Earth is evidently getting worse. While high-density constellations intrinsically increase the risk of satellite collisions, a key observation is that they can also be used to mitigate the debris problem. It is evident that to maximize the physical safety of upcoming high-density satellite constellations, a tight integration between space-based and ground-based radars is crucial to provide a more versatile contingency if some part of the detection system fails for some reason. From this perspective, the proposed SBRC concept can be seen as a supporting concept rather than aiming at replacing the legacy space surveillance system.

Space-borne debris detection provides inherent detection flexibility as detection range can be significantly reduced compared to ground-based detection. However, also the transmission power and antenna size must be reduced. In practice, the satellites cannot be brought arbitrarily close to each other due to cost, safety, and interference regulations. Fortunately, this can be mitigated by introducing satellite cooperation for debris detection. The superior performance of a space-borne radar to detect small debris is dependent on the event that

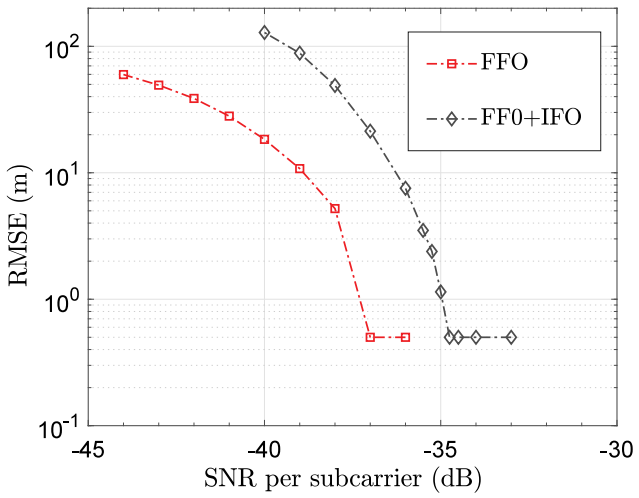

(a) Range estimation.

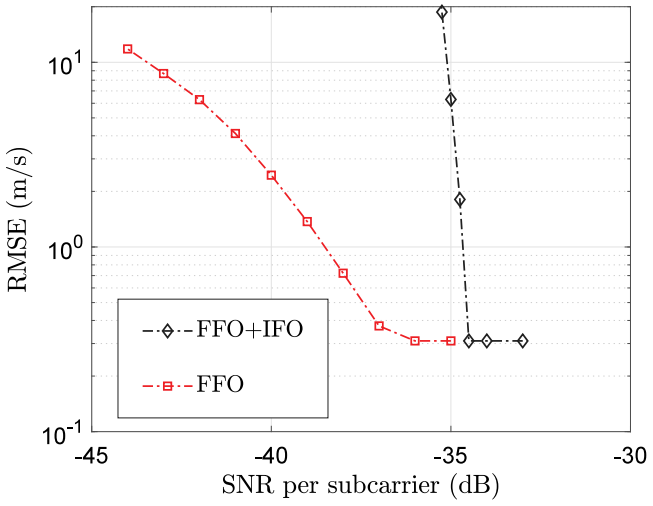

(b) Velocity estimation.

Fig. 8. Simulated RMSE of range and velocity estimations using the proposed 5G-SBRC concept (5G 100 mode). The results saturates to the theoretical lower bounds given in Table 4.

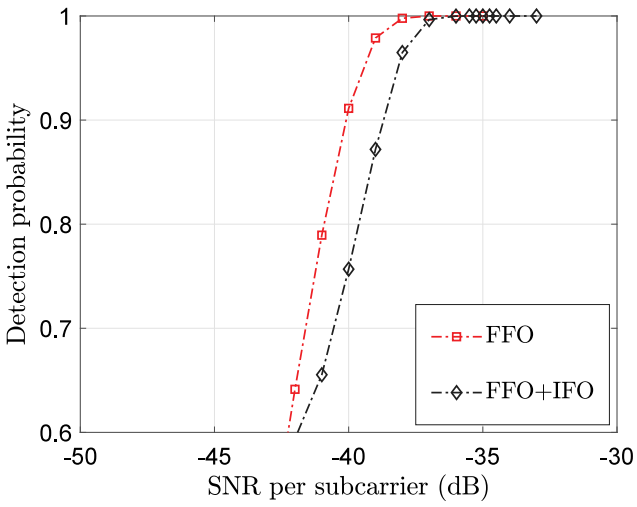

(a) Detection probability vs. SNR per subcarrier.

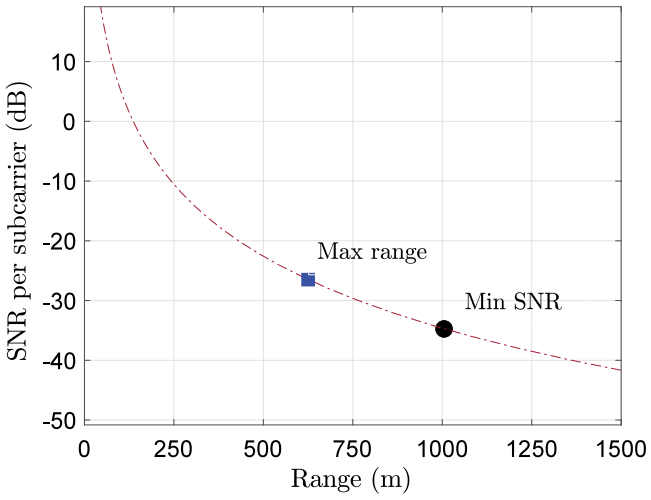

(b) SNR per subcarrier vs. range.

Fig. 9. Achievable detection performance and range for debris diameter of 1 mm using the proposed 5G-SBRC concept (5G 100 mode).

debris becomes relatively close to the radar. We relaxed this assumption and evaluated the case where debris object is randomly placed in the target orbit and evaluated the detection performance. To this extent, we evaluated the effect of the number of satellites and planes for detection performance of small debris. It is found that constellation sizes of 10 000 satellites could provide good detection performance when operating in a stand-alone cooperative mode and target small debris detection in the range of 1–10 mm. This is in line with the upcoming plans of having even 40 000 satellites within a single satellite operator such as SpaceX. Naturally, even lower density satellite constellations can provide significant support to legacy ground-based debris detection radars in the long run. The cooperative detection inherently improves the reliability of the system.

Terrestrial 5G networks are now being integrated into satellite communications and it is, therefore, a good signaling candidate for the proposed SBRC concept. However, we observed that 5G signal structure possesses severe limitations in estimating velocity of debris objects up to 15 km/s which is 100 times higher relative speed than that of typical terrestrial vehicular radar applications. To address this significant problem, we propose a novel Doppler offset compensation approach to mitigate such velocity limitations. The main benefit of the approach is that the compensation can be done jointly with the range and velocity estimations.

Our present performance studies have omitted some interesting aspects, such as practical beamforming algorithms and detailed debris information sharing protocols between satellites, which deserve more attention in the future work along with experimental verifications beyond the conducted simulation studies. Moreover, we have limited our study on space-based radar sensing over communication signals to enable ready-made compatibility with 5G signals. An interesting future topic is also to design next generation SBRC signals that optimize jointly the different objectives of communications and debris detection as well as a tighter integration between space-based and ground-based radars without such compatibility restrictions.

Declaration of competing interest

The authors declare that they have no known competing financial interests or personal relationships that could have appeared to influence the work reported in this paper.

Acknowledgments

The work was funded by VTT Technical Research Centre of Finland through the internal Space For Earth and Extractor projects and in part by Business Finland through the 6G_Sat project. Comments from Szymon Wiktorowicz, Tero Kiuru, Pekka Rantakari, Mervi Hirvonen, and Ilkka Moilanen are acknowledged.

References

[1] ESA, space debris by the numbers, 2020, https://www.esa.int/Safety_Security/Space_Debris/Space_debris_by_the_numbers, Accessed: 2020-11-9.
[2] Spacenews, space traffic management idling in the first year, 2020, https://spacenews.com/space-traffic-management-idling-in-first-gear/, Accessed: 2020-11-9.
[3] A. Murtaza, S. Pirzada, T. Xu, L. Jianwei, Orbital debris threat for space sustainability and way forward, IEEE Access 8 (2020) 61000–61019.
[4] S. May, S. Gehly, B. Carter, S. Fiegel, Space debris collision probability analysis for proposed global broadband constellations, Acta Astronaut. 151 (2018) 445–455.
[5] C. Mark, S. Kamath, Review of active space debris removal methods, Space Policy 47 (2019) 194–206.
[6] T. Mulelhaupt, et al., Understanding space debris: Causes, mitigation and issues, Crosslink 16 (2015) 1–61.
[7] H. Klinkrad, Space Debris: Models and Risk Analysis, Springer, 2006.
[8] J. Xi, et al., Space debris detection using feature learning of candidate regions in optical image sequences, IEEE Access 8 (220) 150864–150877.
[9] H. Zhao, X. Fu, M. Gao, S. Ding, Research on the visibility of low-orbit debris using space-borne radar, IET Commun. 9 (1) (2015) 31–37.
[10] L. Felicetti, M. Emami, A multi-spacecraft formation approach to space debris surveillance, Acta Astronaut. 127 (2016) 491–504.
[11] D. Cerutti-Maori, et al., Preliminary concept of a space-based radar for detecting MM-size space debris, in: Proc. 7th European Conf. Space Debris, Darmstadt, Germany, 2017, pp. 1–12.
[12] C. Strum, W. Wiesbeck, Wafeform design and signal processing aspects for fusion of wireless communications and radar sensing, IEEE Proc. 99 (7) (2011) 1236–1259.
[13] F. Liu, et al., Joint radar and communication design: Applications, state-of-the-art, and the road ahead, IEEE Trans. Commun. 68 (6) (2020) 3834–3862.
[14] V. Petrov, et al., On unified vehicular communications abd radar sensing in millimeter-wave and low terahertz bands, IEEE Wireless Commun. 26 (3) (2019) 146–153.
[15] M. Kiviranta, I. Moilanen, J. Roivainen, 5G radar: Scenarios, numerology, and simulations, in: Proc. Int. Conf. Military Commun. and Inf. Sys., Budva, Montenegro, 2019, pp. 1–6.
[16] C. Barneto, et al., Full-duplex OFDM radar with LTE and 5G NR waveforms: Challenges, Solutions, and measurements, IEEE Trans. Microwave Theory Techn. 67 (10) (2019) 4042–4054.
[17] A. Guidotti, et al., Architectures and key technical challenges for 5g systems incorporating satellites, IEEE Trans. Veh. Tech. 68 (3) (2019) 2624–2639.
[18] G. Giambene, S. Kota, P. Pillai, Satellite-5G integration: A network perspective, IEEE Netw. 32 (5) (2018) 25–31.
[19] I. Portillo, B. Cameron, E. Grawley, A technical comparison of three low earth orbit satellite constellation systems to provide global broadband, Acta Astronaut. 159 (2019) 123–135.
[20] M. Höyhtyä, M. Corici, S. Covaci, M. Cuta, 5G and beyond for new space: Vision and research challenges, in: Proc. Int. Commun. Sat. Sys., Okinawa, Japan, 2019, pp. 1–8.
[21] O. Kodheli, et al., Satellite communications in the new space era: A survey and future challenges, IEEE Commun. Surveys Tut. 23 (1) (2021) 70–109.
[22] F. Rinaldi, et al., Non-terrestrial networks in 5g and beyond: A survey, IEEE Access 8 (2020) 165178–165200.
[23] B. Mahafza, Radar Systems Analysis and Design using Matlab, CRC Press, 2013.
[24] E. Ekici, I. Akyildiz, M. Bender, A distributed routing algorithm for datagram traffic in LEO satellite networks, IEEE Trans. Netw. 9 (2) (2001) 137–147.
[25] T. Pollet, M. Bladel, M. Moeneclaey, BER sensitivity of OFDM systems to carrier frequency offset and Wiener phase noise, IEEE Trans. Commun. 43 (234) (1995) 191–193.
[26] T. Hwang, et al., OFDM and its wireless applications: A survey, IEEE Trans. Veh. Tech. 58 (4) (2009) 1673–1694.
[27] R. Tikrek, et al., OFDM signals as the radar waveform to solve doppler ambiguity, IEEE Trans. Aerosp. Electron. Syst. 48 (1) (2012) 130–143.
[28] M. Braun, OFDM Radar Algorithms in Mobile Communication Networks (Ph.D. dissertation), Karlsruhe Inst. Technol., Karlsruhe, Germany, 2014.
[29] M. Richards, Fundamental of Radar Signal Processing, McGraw-Hill, New York, 2005.
[30] S. Alfano, D. Negron, J. Moore, Rapid determination of satellite visibility periods, J. Astronaut. Sci. 40 (2) (1992) 281–296.
[31] H. Lim, D. Yoon, Refinements of binary integration for swerling target fluctuations, IEEE Trans. Aerosp. Electron. Syst. 55 (2) (2019) 1032–1036.
[32] M. Braun, et al., Maximum likelihood speed and distance estimation for OFDM radar, in: Proc. IEEE Radar Conf., Washington, USA, 2010, pp. 256–261.
[33] D. Toumpakaris, Estimation of integer carrier frequency offset in OFDM systems based on the maximum likelihood principle, IEEE Trans. Broadcast. 55 (1) (2009) 95–108.
[34] D. Rife, R. Boorstyn, Single tone parameter estimation from discrete-time observations, IEEE Trans. Inform. Theory 20 (5) (1974) 591–598.